JOURNAL OF PROPULSION AND POWER
Vol. 19, No. 1, January–February 2003

Numerical Simulation of Distributed Combustion in Solid Rocket Motors with Metalized Propellant

Jayant S. Sabnis*
Pratt and Whitney, United Technologies Corporation, East Hartford, Connecticut 06108

An Eulerian–Lagrangian two-phase approach suitable for the numerical simulation of the multiphase reacting internal flow in a solid rocket motor with a metalized propellant is discussed. An Eulerian description has been used to analyze the motion of the continuous phase that includes the gas as well as the small (micrometer-sized) particulates, while a Lagrangian description is used for the analysis of the discrete phase that consists of the larger particulates in the motor chamber. An empirical model is used to compute the combustion rate for agglomerates, whereas the continuous-phase chemistry is treated using chemical equilibrium. A computer code incorporating this analysis was used to simulate the reacting flow in a solid rocket motor with an ammonium perchlorate (AP)/hydroxyl terminated polybutadiene (HTPB)/aluminum (Al) propellant. The computed results indicate that the relatively slow combustion rate of aluminum droplets can result in an extended combustion zone in the chamber rather than a thin reaction region. The presence of the extended combustion zone results in the chamber flowfield being far from isothermal and the chemical composition being far from uniform, as would be predicted by a surface combustion assumption. The temperature in the chamber increases from about 2600 K at the propellant surface to about 3550 K in the core. Similarly the chemical composition and the density of the propellant gas also show spatially nonuniform distribution in the chamber. The analysis discussed provides a more sophisticated tool for solid rocket internal flow predictions than is presently available and can be useful in studying apparent anomalies and improving the simple correlations currently in use.

Nomenclature

C_D = drag coefficient
F = total force acting on the particle
$\boldsymbol{F}_D$ = drag force per unit volume acting on the continuous phase
h = enthalpy
$[J]$ = Jacobian matrix of coordinate transformation
m = mass
m_v = rate of mass addition per unit volume to the continuous phase
Nu = Nusselt number
Pr = Prandlt number
p = pressure
$\boldsymbol{q}$ = heat flux vector in the continuous phase
q_v = rate of interphase heat transfer to the continuous phase
Re = Reynolds number
St = Stokes number
T = temperature
t = time
U = velocity
w = rate of production per unit volume due to chemical reaction
x_i = components of position vector in physical space
Y = elemental mass fraction
Y^S = species mass fraction
y^j = components of position vector in coordinate space
α = void fraction
α_{ki} = mass fraction of element k in species i
κ = thermal conductivity
μ = viscosity
ρ = density
τ = stress tensor
Φ = viscous dissipation

Subscripts

i = species i
k = element k
p = discrete phase
R = relative

Received 9 October 2001; revision received 1 October 2002; accepted for publication 3 October 2002.

*Director, Aerodynamics. Associate Fellow AIAA.

Introduction

SIMULATION of the internal flow in solid propellant rocket motors has been the subject of several previous research studies due to the impact of the flowfield on motor performance and reliability. An understanding of the internal flow is vital to the design of the insulation, improvement of the combustion stability, minimization of the slag accumulation, etc. Previously used predictive techniques include potential flow analyses coupled with iterative boundary-layer corrections, as well as the rotational flow analysis of Culick.[1] Numerical solution of ensemble-averaged Navier–Stokes equations has been utilized by several researchers recently in view of the generality of this approach and the recent advances in numerical techniques as well as the digital computers. Multidimensional numerical analyses have been developed to simulate single-phase, nonreacting flow (for example, Sabnis et al.[2] and Chang[3]) as well as two-phase nonreacting flow (for example, Madabhushi et al.[4] and Golafshani and Loh[5]). However, predictive capabilities for simulation of the solid rocket internal flow including the distributed combustion are limited.

In modeling the combustion in solid rocket motors, one must consider the effect of metals used in the propellant formulation on the combustion process. Metals are used in solid propellants commonly to increase specific impulse because they burn with high temperatures without any adverse effects on the detonation characteristics of the propellant. The physics of metal combustion, however, is very different from that of other propellant ingredients. Hence, the combustion characteristics of metalized propellants can be significantly different. Several different metals have been considered and used in solid propellants with aluminum being extensively used in mass fractions of 12–22% (Ref. 6). Although the modeling approach is discussed here for aluminized propellants, it is quite general and can be applied to other metalized propellants.

During the combustion of aluminized propellant, the aluminum particles in the propellant melt and form liquid aluminum at the burning propellant surface. Because of the physical properties of aluminum and its oxide, a large fraction of aluminum remains unreacted and in liquid state at the burning propellant surface. Several liquid droplets coalesce into large "agglomerates" (often on the order of 100–200 μm). These agglomorates leave the propellant surface and continue to burn relatively slowly due to low volatility of aluminum as they traverse the motor chamber. The vaporized aluminum reacts with the oxidizing species in the gas phase forming aluminum oxide. Whereas most of this aluminum oxide "smoke" diffuses outward into the flowfield, a part is captured on the agglomorate surface and condenses to form an oxide shell. The formation of aluminum oxide shell on the surface of the droplet further contributes to the "slowness" of aluminum combustion. By comparison, the reaction rate for the remaining propellant constituents is rapid and it is generally accepted (for example, Price[6]) that the combustion of aluminum droplets in the motor chamber is diffusion controlled (or, to be more precise, mass transfer controlled). Note that the gaseous-phase flowfield would in general be chemically reacting and that its composition would change due to changes in thermodynamic state, as well as the combustion of the unburned aluminum. The physics of aluminum combustion also results in a bimodal distribution of aluminum oxide representing the smoke and the "caps," which are on the order 1.5 and 100 μm in size, respectively. To model this flowfield, the analysis must include capability to account for multiple phases, as well as effects of all of the chemical reactions.

Computational techniques used in simulation of two-phase flows can be broadly categorized into two approaches, namely, the Eulerian–Eulerian analysis and the Eulerian–Lagrangian analysis. Both techniques involve computing the continuous phase using an Eulerian analysis. The influence of the discrete phase (either solid particles or liquid droplets) on the continuous phase is accounted for by inclusion of interphase coupling terms in the Eulerian equations, which in the absence of these terms would be the usual Navier–Stokes equations. The discrete phase, on the other hand, may be treated with either a continuum or a discrete model. The Eulerian–Eulerian technique uses a continuum model for the discrete phase and is commonly termed the two-fluid model. This approach models a dense granular bed very conveniently, and this undoubtedly accounts for its popularity in modeling gun interior ballistics, where large particle loading ratios occur over most of the cycle (for example, Gough[7] and Gibeling et al.[8]). The Eulerian–Lagrangian approach employs a Lagrangian description to analyze the motion of the discrete phase, using computational "particles" to represent a collection of physical particles (or droplets). Newton's law of motion is employed to simulate the particle motion under the influence of the local environment produced by the continuous phase. The discrete-phase attributes (such as the position and velocity vectors, size, temperature, composition, etc.) are updated along the trajectories. Because the particulate size and composition are attributes assigned to the computational particles, it is easy to account for changes in particle size and composition due to combustion, etc.

In simulation of solid rocket internal flows, it is necessary to account for the fact that the burning aluminum droplets (which constitute the discrete phase) are not monodispersed and, furthermore, that the chemical composition of all of the droplets is not the same. To accomplish this in the Eulerian–Eulerian methodology, the two-fluid model can be generalized into a multifluid model. However, the CPU time requirements increase rapidly with increasing number of particle size classes because an extra fluid has to be added for every particle class (representing particles with similar size, composition, etc.), thereby increasing the number of partial differential equations. The CPU time increase is particularly dramatic if implicit schemes are retained in view of their improved stability bounds and efficiency with multiple length scales. With the Eulerian–Eulerian methodology, the numerical dissipation and dispersion effect could be a major problem in the discrete phase, where it might be necessary to retain sharp inter-phase boundaries. Also, it seems evident from existing experimental work that the use of an effective particle Schmidt number depending only on local conditions, such as is currently done in the two-fluid model, would be erroneous for larger particles.

The Eulerian–Lagrangian analysis treats the particle size and composition as one of the attributes assigned to computational particles and, hence, can easily account for changes in particle size and composition due to combustion, etc., and more economically than would be possible with an Eulerian–Eulerian analysis. Furthermore, this approach involves integration of ordinary differential equations (ODE) for the discrete phase and, hence, is numerically efficient in addition to eliminating the numerical dissipation. The deterministic nature of the particle dynamics allows the incorporation of models for turbulent dispersion, agglomeration, collision, etc. Note that it should, in principle, be possible to include elements of the physics of the Lagrangian particle description in the two-fluid model, and this might be a necessary development to adequately describe certain two-phase flows using a two-fluid model.

In Eulerian–Lagrangian algorithms, the interphase coupling terms for the continuous-phase equations can be computed using a particle trajectory approach or a particle distribution approach. In the particle trajectory approach, the coupling terms are computed from the knowledge of the trajectories for representative particles and their attributes at the intersection of the trajectories with the Eulerian cell boundaries. In the particle distribution approach, the coupling terms are computed from the instantaneous distribution of the particles in the computational domain. The trajectory approach has been employed, for example, by Crowe et al.[9] and Gosman and Ioannides,[10] and the particle distribution approach has been utilized by Dukowicz[11] and Sabnis et al.[12] In the algorithms based on the trajectory approach, the integration of the Lagrangian equation of motion for representative particles is carried out starting from the injection location until the particle either leaves the computational domain or evaporates to a negligible size. During this interaction, the continuous-phase flowfield is held frozen. The interphase coupling terms for the continuous-phase conservation equations are computed for every Eulerian cell from the net influx of the appropriate dependent variable into the Eulerian cell, due to all trajectories intersecting the particular Eulerian cell. For example, the source term for the continuity equation is obtained as the total mass of the discrete phase entering the cell along all trajectories minus the total discrete-phase mass leaving the cell along all trajectories. The coupling terms thus computed are used to calculate the continuous-phase flowfield that can then be used to reevaluate the trajectories and the source terms. This iterative process is continued until the desired level of convergence is achieved. These algorithms are, thus, inherently unsuitable for transient calculations, and furthermore, the global iteration procedure used can require substantial computer time. In the particle distribution approach, such as that used by Dukowicz[11] and Sabnis et al.,[12] the source terms are computed from the instantaneous interaction between the continuous phase and all of the particles in the particular Eulerian cell. Thus, the source term for the continuous-phase continuity equation, for example, is given by the sum of evaporation rates for all of the droplets in the cell. The calculation procedure consists of updating the particle distribution through one time step followed by updating the continuous-phase flowfield through one time step. In general, it is not necessary that the time step used to integrate the particle motion and that used in updating the continuous-phase flowfield be equal. However, by making the two time steps equal, the particle distribution algorithms can be used for simulation of transient phenomena. If only a steady-state solution is desired, then the two time steps can be made unequal, and matrix preconditioning techniques can be used for convergence acceleration.

The reacting multiphase flow in the solid rocket chamber can be effectively treated as consisting of a continuous phase composed of the products of combustion from the binder, the ammonium perchlorate (AP), and reacted aluminum, and a discrete phase composed of particles containing aluminum and Al_2O_3. The governing equations for such an analysis were formulated by Sabnis et al.[13] and applied to simulate the multiphase reacting flow in a solid rocket motor with a metalized propellant. The details of this analysis and its application to a test case are discussed.

Analysis and Governing Equations

As discussed earlier, the physics of metalized propellant combustion includes diffusion transfer controlled combustion of agglomerates as well as gas-phase reactions. The kinetic timescales associated with the reactions in the continuous phase, however, are likely to be small compared to the fluid dynamic timescales in the chamber. The continuous-phase chemistry can, therefore, be treated using chemical equilibrium. Empirical correlations can be used to simulate the diffusion controlled distributed combustion of the aluminum droplets and chemical equilibrium to simulate the gas-phase chemistry in modeling the solid rocket internal flow. Combustion of aluminum also results in a bimodal distribution of Al_2O_3 particulates in the motor chamber, small-sized particles that are on the order 1.5 μm (frequently called the smoke) and larger-sized particulates that are on the order 100 μm (frequently called the caps).

The flowfield in the combustion chamber can be modeled as consisting of two "phases": a continuous phase consisting of the combustion products from AP, the binder, as well as reacted aluminum, and a discrete phase consisting of the aluminum droplets with Al_2O_3 caps. The continuous phase in this model includes Al_2O_3 smoke, that is, small-sized droplets/particulates, and the discrete phase includes larger-sized agglomerates consisting of aluminum as well as Al_2O_3. The distinction between the continuous and the discrete phases is based on the approach used to simulate the dynamics of the respective phase rather than the thermodynamic phase, that is, solid, liquid, or gas. The choice of the approach used to simulate the dynamics does depend on the specific problem under consideration, and hence, the analysis has been kept general enough to provide this flexibility. For example, if coalescence of micrometer-sized particles with the larger particles were to be studied, it would not be possible to include the micrometer-sized particles as a part of the continuous phase, and both types of particulates would be treated as a part of the discrete phase. Because the objective of this analysis is to simulate the distributed combustion of aluminum, the Al_2O_3 smoke particles (which are in equilibrium with the gas) are considered a part of the continuous phase. Combustion of the aluminum in the discrete phase consisting of larger sized agglomerates results in mass addition to the continuous phase, whereas surface oxidation and capture of Al_2O_3 smoke by the droplets results in mass depletion from the continuous phase. Both of these effects are modeled using empirical correlations, and the net sum represents interphase mass transfer.

The CELMINT code that incorporates the analysis discussed herein solves the ensemble-averaged Navier–Stokes equations with droplet mass, momentum, and energy interchange source terms determined from the Lagrangian droplet transport calculation. The governing Eulerian equations are written in a general nonorthogonal, body-fitted coordinate system. The equations to be solved are continuity, momentum conservation, energy conservation, species transport, and turbulence model equations. The turbulence model used in the present calculations is the transitional two-equation (k–ε) model of Jones and Launder,[14] along with the modifications discussed by Sabnis et al.[15] for injection-driven flows. The vector form of the equations with the droplet mass, momentum, and energy interchange terms is presented next.

Continuous-Phase Analysis

The global mass, momentum, and energy conservation equations for the continuous phase can be written as

$$\frac{\partial(\alpha\rho)}{\partial t} + \nabla\cdot(\alpha\rho\boldsymbol{U}) = m_v \tag{1}$$

$$\frac{\partial(\alpha\rho\boldsymbol{U})}{\partial t} + \nabla\cdot(\alpha\rho\boldsymbol{U}\boldsymbol{U}) = -\nabla(\alpha p) + \nabla\cdot(\alpha\tau) + m_v\boldsymbol{U}_p + \boldsymbol{F}_D \tag{2}$$

$$\frac{\partial(\alpha\rho h)}{\partial t} + \nabla\cdot(\alpha\rho\boldsymbol{U}h) = \alpha\frac{\mathrm{D}p}{\mathrm{D}t} + \alpha\Phi - \nabla\cdot(\alpha\boldsymbol{q}) + q_v - \boldsymbol{U}_p\cdot\boldsymbol{F}_D + m_v\left(h_v + \frac{1}{2}\boldsymbol{U}_R\cdot\boldsymbol{U}_R\right) \tag{3}$$

where m_v is the rate of mass addition per unit volume due to interphase mass exchange, $\boldsymbol{U}_P$ is the particle velocity, τ is the stress tensor (molecular and turbulent), q_v is the rate of heat transfer per unit volume to the continuous phase, $\boldsymbol{U}_R$ is the velocity of continuous phase relative to the discrete phase, and h_v is the vapor enthalpy for the discrete phase. Note that all of the discrete-phase source terms, that is, m_v, $m_v\boldsymbol{U}_p$, $\boldsymbol{F}_D$, q_v, etc., and the void fraction α in the preceding equations are computed for each computational cell by summation of the appropriate quantities over all of the computational particles within the cell. The mixture enthalpy h is defined as

$$h = \sum_{i=1}^{n} Y_i^s h_i \tag{4}$$

where Y_i^s is the mass fraction of species i, n is the number of species, and h_i is the enthalpy of species i, which can be evaluated from the polynomial

$$h_i = h_i^0 + \sum_{j=1}^{5} a_{ij}T^j \tag{5}$$

The heat flux vector $\boldsymbol{q}$ is given by

$$\boldsymbol{q} = -\kappa\nabla T + \sum_{i=1}^{n} h_i\rho D_i\nabla Y_i^s \tag{6}$$

The second term in the expression for the heat flux vector represents the interdiffusional energy flux. This expression can be simplified significantly if the laminar and turbulent Lewis numbers are assumed to be unity, to yield

$$\boldsymbol{q} = -(\mu_\ell/Pr_\ell + \mu_T/Pr_T)\nabla h \tag{7}$$

The governing equations for the species transport can be written as

$$\frac{\partial\left(\rho Y_i^s\right)}{\partial t} + \nabla\cdot\left(\rho\boldsymbol{U}Y_i^s\right) = \nabla\cdot\left(\rho D_i\nabla Y_i^s\right) + w_i + m_{v_i} \qquad i = 1, 2, \ldots, n \tag{8}$$

where D_i and w_i are the diffusion coefficient and the rate of production due to chemical reaction, respectively, for species i, and m_{vi} is the rate of mass addition for species i (per unit volume) due to interphase mass exchange. Note that designating Al and Al_2O_3 as species 1 and 2, respectively, yields $m_{vi} \equiv 0$ for $i > 2$ because the discrete phase is assumed to consist of Al and Al_2O_3 only.

The number of species present in the combustion chamber can be quite large, even if the species present in trace quantities are to be neglected. Thus, the computational effort required to solve the species equations can be formidable. Hence, the present formulation has used the Shvab–Zeldovich transformation as follows. The mass fraction of element k in species i is defined as α_{ki} so that

$$\sum_{k=1}^{\ell}\alpha_{ki} = 1 \tag{9}$$

where ℓ is number of elements, and

$$\sum_{i=1}^{n}\alpha_{ki}Y_i^s = Y_k$$

is the mass fraction of element k in gas. Note that because the chemical reactions do not result in production or destruction of elements,

$$\sum_{i=1}^{n}\alpha_{ki}w_i = 0 \tag{10}$$

Furthermore, designating aluminum and oxygen as elements 1 and 2, respectively, results in $\alpha_{11} = 1$, $\alpha_{12} = \frac{27}{51}$, $\alpha_{21} = 0$, and $\alpha_{22} = \frac{24}{51}$,

whereas $\alpha_{k1} \equiv \alpha_{k2} \equiv 0$ for $k > 2$. If the diffusivities D_i for species are assumed to be equal, the n species transport equations can be reduced to the following elemental transport equations for the ℓ elements:

$$\frac{\partial(\rho Y_k)}{\partial t} + \nabla \cdot (\rho \boldsymbol{U} Y_k) = \nabla \cdot (\rho D \nabla Y_k) + \sum_i \alpha_{ki} m_{v_i},$$

$$k = 1, 2, \ldots, \ell \quad (11)$$

Note that for $k > 2$, the elemental transport equations do not have any source terms. Thus, the elemental transport equations for elements 3–ℓ are self-similar. Because the global continuity equation is being solved, one equation from the elemental transport equations need not be solved, and it is convenient to select the self-similar equations for this purpose. Thus, only two equations for the elemental transport have to be solved. Also, if the rate of accumulation of Al_2O_3 in the particle were proportional to the combustion rate, that is, m_{v1} and m_{v2} were to be proportional to each other, only one elemental transport equation would have to be solved.

The governing equations discussed can be used to compute the thermodynamic state and the elemental composition of the continuous phase. Because the reaction rates in the continuous phase are assumed to be rapid, the chemical composition of the mixture can be obtained from chemical equilibrium calculations. If the chemical equilibrium calculations were to be carried out at every grid point for every time step, the computational effort could be very significant. Hence, tabular data for the gas-phase composition as a function of the elemental aluminum mass fraction in the continuous phase and the continuous-phase enthalpy can be generated using a suitable chemical equilibrium code, such as the CET86 code of Gordon and McBride.[16] These tables can be used with an interpolation scheme to determine the chemical composition of the continuous phase corresponding to the enthalpy and aluminum mass fraction at every grid point during the calculations.

The conservation equations discussed above are solved using a consistently split, linearized block-implicit (LBI) numerical scheme developed by Briley and McDonald.[17] The LBI scheme for scalar convection and diffusion in two space dimensions does not suffer from a stability restriction that relates the temporal step to the spatial mesh size. This is an important advantage, apparently retained for the present system of equations, in view of the existence of high characteristic velocities and the need to use locally refined meshes for accurate solution of the flowfield equations in the regions of sharp velocity, temperature, or species concentration gradients. The solution procedure treats the nonlinearities noniteratively by Taylor series linearization in time and then splitting the matrix into a sequence of easily solved block-banded subsystems. The solution procedure is, thus, computationally efficient. The LBI algorithm has been found to be rapidly convergent and conditionally stable in three dimensions for nonperiodic inflow and outflow boundary conditions. Details of the stability and convergence rate of the algorithm have been discussed by Briley et al.[18]

The boundary conditions to be used with the continuous-phase governing equations are as follows. The head end and the nozzle walls are considered adiabatic and chemically inert. Hence, the velocity components and the normal derivatives of enthalpy and the elemental mass fractions at these walls are set to zero. The nozzle exit boundary is a supersonic outflow boundary (except in the boundary layer), and hence, all of the dependent variables at this boundary are linearly extrapolated. At the propellant surface, the continuous-phase mass flux is determined from the propellant burn rate, and the temperature is determined by the adiabatic flame temperature for the propellant formulation. Note that the continuous-phase mass flux must be corrected to account for the discrete-phase mass flux to be used in the discrete-phase analysis, and similarly the adiabatic flame temperature calculations must also account for the energy required to melt the corresponding mass of aluminum and raise it to the flame temperature. The elemental composition of the continuous phase at the propellant surface is also determined from the propellant composition and the assumption regarding the fraction of aluminum to be included in the continuous phase at the propellant surface.

Discrete-Phase Analysis

The interphase source terms in the continuous-phase governing equations [Eqs. (1–3)] are obtained from the discrete-phase analysis, which uses a Lagrangian description for the motion of computational particles. Each computational particle represents a collection of physical particles that have the same attributes (such as spatial location, velocity, mass, size, composition, temperature, etc.). This representation of a group of physical particles by a computational particle is similar to the representation of a group of molecules by a computational particle in direct simulation Monte Carlo methods (cf., Bird[19]).

The equation of motion for a particle can be written in the form

$$\frac{\mathrm{d}^2 \boldsymbol{X}}{\mathrm{d}t^2} = \frac{\boldsymbol{F}}{m} \quad (12)$$

where $\boldsymbol{X}$ is the position vector of the particle and m is the particle mass. In general, $\boldsymbol{F}$ contains "body" forces, such as those due to gravity or electromagnetic fields, and the force acted on the particle by the fluid, $\boldsymbol{F}_D$. Integration of Eq. (12) yields

$$\frac{\mathrm{d}\boldsymbol{X}}{\mathrm{d}t} = \int_{t_0}^{t} \frac{\boldsymbol{F}}{m}\,\mathrm{d}\tau + \left.\frac{\mathrm{d}\boldsymbol{X}}{dt}\right|_{t_0} \quad (13)$$

At this stage, a coordinate transformation $\boldsymbol{Y} = \boldsymbol{Y}(\boldsymbol{X})$ is introduced to transform the equation of motion into the computational coordinate space corresponding to the Eulerian analysis for the continuous phase, that is,

$$y^j = y^j(x_1, x_2, x_3) \quad (14)$$

where y^j are the computational coordinates (the components of $\boldsymbol{Y}$) used in the Eulerian analysis of the continuum phase and x_i are the physical coordinates (the components of $\boldsymbol{X}$). Let $\boldsymbol{J}$ be the inverse of the transformation matrix, that is, let $\boldsymbol{J}$ be the matrix with elements J_{ij}, where

$$J_{ij} = \frac{\partial y^i}{\partial x_j}$$

Then,

$$\frac{\mathrm{d}\boldsymbol{Y}}{\mathrm{d}t} = \boldsymbol{J}\frac{\mathrm{d}\boldsymbol{X}}{\mathrm{d}t} \quad (15)$$

Substituting Eq. (15) into Eq. (13) yields

$$\frac{\mathrm{d}\boldsymbol{Y}}{\mathrm{d}t} = \boldsymbol{J}\int_{t_0}^{t} \frac{\boldsymbol{F}}{m}\,\mathrm{d}\tau + \boldsymbol{J}\left.\frac{\mathrm{d}\boldsymbol{X}}{\mathrm{d}t}\right|_{t_0} \quad (16)$$

Integration of the preceding equation allows tracking of the particle motion in computational coordinate space. This approach offers some very significant advantages. Because the motion of the particle is tracked in the computational coordinate space, no searching is needed to determine which Eulerian grid point will be affected by a particular particle via the source terms. Also, tracking the motion in the computational space allows the estimate of the time taken by the particle to cross the boundaries of the Eulerian cell where it currently resides. This estimate is used in the selection of subtime steps (described later) used in integrating the equation of motion. Similarly, the search for boundaries is simplified, making it easier to determine whether a particle has reached a solid boundary and should be reflected, or a particle has left the computational domain and should be omitted. This latter advantage is of major importance when the number of boundaries is large.

In the CELMINT formulation, the time step for the particle motion, Δt_p, is not necessarily the same as the time step Δt_e used in the

Eulerian equations, and this feature can be used to accelerate convergence for steady flow problems. For transient flow problems, caution must be exercised to ensure consistency between the discrete- and continuous-phase equations. The time step Δt_p is defined as a specified fraction of the characteristic evaporation time of the system, that is, the time for all of the particulate mass in the system to be replaced. During the time period Δt_p, particles are moved through the domain by integrating their Lagrangian equations of motion using a sequence of subtime steps Δt_s, during which the gas-phase flow properties are assumed known from the previous Eulerian time step calculation. The subtime steps are chosen as the minimum time for the particle to cross the nearest Eulerian cell boundary and a kinematic timescale defined as a fraction, for example, 0.1, of the ratio of particle velocity to acceleration. Note that for accuracy, the maximum allowable subtime step could be significantly different for different particles depending on their location, mass, etc. The subtime step approach has been adopted to provide an accurate representation of the particle motion because at the end of each subtime step the drag force, evaporation rate, and heat transfer are updated using the latest particle attributes as well as the continuous-phase values corresponding to the new particle locations.

Injection Modeling

The injection process is simulated by introducing a predetermined number of pulses of new computational particles at the appropriate locations during the period Δt_p. The injected particles are then moved through the computational domain using a sequence of subtime steps until the end of the time period Δt_p is reached. The total mass flow rate of the discrete phase is normally known and is used in computing the particulate mass injected during each pulse. The propellant burn rate and the mass fraction of aluminum in the propellant determine the mass flow rate of the particulates for the injection process. The size of the injected droplets is computed stochastically using a log-normal size distribution with a specified mean and standard deviation, which is then used to compute the statistical weight associated with, that is, the number of physical particles represented by, the computational particle. The particle size distribution in solid rockets has been the subject of previous studies due to its importance on slag formation, etc. Salita[20] has analyzed data from three aluminized propellants and found the size distribution to be log-normal and bimodal. Typical values of the mass-mean diameter were about 1.5 μm for the micrometer-sized smoke and about 100 μm for the larger particles with $\log_{10}$ standard deviation being 0.2. The micrometer-sized particles accounted for as much as 80% of Al_2O_3 mass.

The particles are injected normal to the propellant surface with a specified velocity. In the calculations of Sabnis et al.,[13] the particle injection velocity was assumed to be 1% of the gas velocity at the propellant surface. Madabhushi et al.[4] have studied the sensitivity of the particle dynamics to the injection velocity by varying the injection velocity between 1 and 25% of the gas velocity. The results of their study show the particle dynamics to be insensitive to the injection velocity.

Interphase Drag and Heat Transfer Models

Models for interphase exchange rates of mass, momentum, and energy are needed in evaluation of the source terms in the governing equations for the continuous phase, as well as in the integration of the equations of particle motion. The CELMINT code maintains these models in a modular form, and they can be readily replaced. This approach makes it possible to incorporate models best suited to the physical problems under consideration. In the calculations of Sabnis et al.,[13] the total force on the particle consisted of the drag force. This drag force on the particle and the rate of heat transfer to the particle can be evaluated via commonly used empirical correlations. Specifically, the drag force $\boldsymbol{F}_D$ on a particle can be computed from

$$\boldsymbol{F}_D = \tfrac{1}{8} C_D \rho \pi D_p^2 |\boldsymbol{U}_R| \boldsymbol{U}_R \tag{17}$$

where D_p is the particle diameter and the drag coefficient C_D is given by[21]

$$C_D = (24/Re_P)\left(1 + 0.15 Re_p^{0.687}\right), \qquad Re_p < 1000$$

$$C_D = 0.438, \qquad Re_p \geq 1000 \tag{18}$$

Here the particle Reynolds number Re_p is given by

$$Re_p = \rho U_R D_p / \mu \tag{19}$$

The heat transfer rate to the particle can be computed from

$$q_p = Nu_p \pi D_p \kappa (T - T_p) \tag{20}$$

where κ is the thermal conductivity of the continuous phase, T_p is the particle temperature, and the Nusselt number Nu_p is related to the Reynolds number Re_p and Prandtl number Pr by[22]

$$Nu_p = 2.0 + 0.6 Re_p^{0.5} Pr^{0.687}, \qquad Re_p \leq 278.92$$

$$Nu_p = 0.37 Re_p^{0.6}, \qquad Re_p > 278.92 \tag{21}$$

Droplet Combustion Model

A droplet combustion model is necessary to evaluate m_{v1} and m_{v2}. A modified form of the correlation provided by Hermsen[23] has been used to evaluate the aluminum combustion rate for the droplets. It is further assumed that a specified fraction of the reacted aluminum results in formation of Al_2O_3 on the surface and is captured in the particle. Thus, the rate of depletion of Al_2O_3 from the continuous phase is proportional to the rate of aluminum mass addition. This assumption results in the two elemental transport equations being proportional to each other and only one need be solved. The Hermsen correlation includes a correction factor R_k to account for augmentation of the combustion rate due to inter-phase slip, etc. Such an approach is necessary with a global model to match the burning time data inferred from test motor firings. However, with the Eulerian–Lagrangian analysis, the local environment of each droplet is known and, hence, can be used in evaluating the burning rate. Because the combustion of the droplets is assumed to be mass transfer controlled, the augmentation of the combustion rate would be a direct consequence of the increased mass transfer due to relative flow. Hence, an empirical correlation that relates the Sherwood number to the Reynolds number can be directly used to evaluate the burning rate augmentation. A similar approach has been utilized previously by King[24] along with simplified flowfield analyses for calculation of metal combustion efficiency in nozzleless solid rocket motors. In the present approach, the Hermsen[23] correlation is rewritten as

$$\frac{\mathrm{d}(m_{\mathrm{Al}})}{\mathrm{d}t} = -\frac{\pi}{2} \rho_{\mathrm{Al}} \frac{k}{n} D_p^{3-n} \tag{22}$$

where the exponent n is 1.8, ρ_{Al} is the density of aluminum, and the burning rate constant k ($\mathrm{cm}^{1.8}/\mathrm{s}$) in Eq. (22) is computed from

$$k = 8.3314 \times 10^{-5} \cdot A_k^{0.9} \cdot p_c^{0.27} \cdot Sh/2 \tag{23}$$

where p_c is the chamber pressure (pounds per square inch absolute), Sh is the Sherwood number based on particle diameter, and A_k is a measure of the availability of oxidizing species and is computed using

$$A_k = 100 \sum_i X_i, \qquad i = \mathrm{CO_2}, \mathrm{H_2O}, \mathrm{O_2}, \mathrm{OH}, \mathrm{O} \tag{24}$$

The Sherwood number can be computed using empirical correlation relating it to the Reynolds number, that is, Eq. (21) with Nusselt number Nu replaced by Sherwood number.

Droplet Breakup and Coalescence Models

The liquid droplets in a solid rocket motor undergo size changes due to breakup and coalescence in addition to combustion. This phenomenon is accounted for in the present methodology by incorporating models to simulate the breakup and coalescence processes. The droplet breakup is caused by the shear force exerted on the droplet

by the continuous phase moving relative to the droplet. The force preventing the droplet breakup is provided by the surface tension effect. Hunter et al.[25] have recommended a critical Weber number criterion for determining when droplet breakup occurs along with an empirical fragmentation factor. The methodology of Hunter et al. was based on the work of Bartlett and Delaney[26] and several other authors, and the interested reader is referred to Hunter et al.[25] for additional details and references. The model essentially states that the maximum droplet radius is controlled by a balance between the aerodynamic viscous force and the surface tension force acting on the droplet. The drag/surface tension relation is written as a critical Weber number condition, that is,

$$We_c = \frac{\rho |\boldsymbol{U}_R|^2 D_p}{\sigma_p} = \frac{4}{C_D} \tag{25}$$

where σ_p is the particle surface tension. The factor of four in Eq. (25) has been used to correct for the nonspherical drop shape, which is known to exist before breakup. As noted by Hunter et al.,[25] Eq. (25) is consistent with the commonly recommended critical Weber number of order 10 when C_D is 0.4. The fragmentation factor is the radius ratio before/after breakup, that is,

$$\Phi = \left\{ \frac{\text{average mass before breakup}}{\text{average mass after breakup}} \right\}^{\frac{1}{3}} \tag{26}$$

The code uses a default value of two for the fragmentation factor. A limited number of runs has been carried out with larger values of Φ (up to 10), and the results of these runs indicate that the particle size distribution at the nozzle exit does not appear to depend strongly on the value of Φ. A larger value of Φ results in fewer breakup events for particles, whereas a smaller value of Φ results in the particle undergoing several more breakup events. Because the breakup of the droplets takes place in a fairly narrow region in the nozzle, the breakup history does not play a significant role.

The coalescence of the Al_2O_3 caps due to particle collisions will result in some growth in the agglomerate size in the motor. Modeling this phenomenon is difficult computationally if large particle collisions have to be treated. However, the available evidence in a rocket motor[27] indicates that the large-particle coalescence efficiency associated with large-particle collisions is only about 5%, whereas the collision of micrometer-size Al_2O_3 smoke particles with the larger agglomerates results in nearly 100% coalescence. Therefore, the current droplet coalescence model does not take into account large-particle collisions. Coalescence due to the collision of smoke particles (which are considered as part of the continuous phase for kinematic purposes) is simulated using a simple sweeping model, in which a certain fraction of smoke particles that flow past a large droplet are assumed to collide and stick to the droplet. The so-called collection efficiency for spherical particles was originally correlated by Hunter et al.[25] and subsequently corrected by Salita.[27] This collection efficiency factor η_c is given by

$$\eta_c = \frac{\mathrm{St}_p^{1.2595}}{1.2615 + \mathrm{St}_p^{1.2595}} \tag{27}$$

where the Stokes number St_p for the particle is given by

$$\mathrm{St}_p = \frac{\rho_s D_s^2 |\boldsymbol{U}_R|}{9 \mu_l D_p} \tag{28}$$

where ρ_s is the smoke density, D_s is the smoke particle diameter, $\boldsymbol{U}_R$ is relative velocity between the continuous and discrete phases, μ_l is the molecular (laminar) viscosity, and D_p is the large-particle diameter.

The mass rate of production of Al_2O_3 in the discrete phase due to coalescence may then be written as

$$\frac{\mathrm{d}\left(m_{\mathrm{Al_2O_3}}\right)_{\mathrm{coa}}}{\mathrm{d}t} = \pi R_p^2 \rho |\boldsymbol{U}_R| Y^s_{\mathrm{Al_2O_3}} \eta_c \tag{29}$$

where $Y^s_{\mathrm{Al_2O_3}}$ is the mass fraction of Al_2O_3 (smoke) in the continuous phase, which is equal to $Y_{\mathrm{Al}}/\alpha_{12}$. Y_{Al} is the mass fraction of elemental aluminum in the continuous phase, whereas α_{12} is the mass fraction of elemental Al in Al_2O_3 [see discussion relating to Eq. (9)].

Discrete-Phase Turbulent Dispersion

In two-phase flows, the continuous-phase turbulence results in dispersion of the discrete phase. This process has been modeled by some researchers[28] by adding a diffusion velocity obtained from some phenomenological model to the particle velocity. In the present analysis, this effect is modeled by evaluating the fluid force on a particle using an instantaneous continuous-phase velocity field rather than a mean velocity field. The instantaneous velocity components were obtained by adding stochastically generated turbulent velocity components to the mean velocity field for the continuous phase. If the continuous-phase turbulence is assumed to be isotropic and the random turbulent velocity components are assumed to have a Gaussian probability distribution, then the standard deviation for the distribution can be shown to be $(2k/3)^{1/2}$, where k is the turbulent kinetic energy. The random turbulent velocity components can, thus, be obtained by sampling a suitable random number.

This technique offers a way to treat the effect of continuous-phase turbulence on the discrete-phase dispersion in a manner that is less empirical than the techniques traditionally used with Eulerian–Eulerian analyses. Similar techniques for modeling the discrete phase turbulent dispersion have been used by, for example, Gosman and Ioannides,[10] Dukowicz,[11] and Hotchkiss.[29]

Application and Results

The CELMINT code incorporating the discussed analysis was used by Sabnis et al.[13] to simulate the internal flow in a cylindrical port solid rocket motor. The geometry was similar to the super Ballistics Test (BATES) motor at the initial grain configuration. The propellant used in these demonstration calculations contained 15% aluminum by weight. Figure 1 shows a schematic of the motor geometry, and the propellant data are listed in Table 1. The computational grid used in these calculations consisted of 60 grid points distributed along the radial direction and 140 grid points distributed along the motor axis. Appropriate near-wall resolution was used to properly resolve the flow gradients at the walls. Figure 2 shows the computational domain and the grid.

The calculations were initiated by specifying the continuous-phase mass flux at the grain surface to match the propellant burn rate and setting the continuous-phase temperature at the propellant surface equal to the flame temperature. To assess the effect of the

Table 1 Propellant data

Property	Value
Composition	
AP	71.00%
Binder (HTPB)	14.00%
AL	15.00%
Density	1794.6 kg/m^3
Burn rate	9.0678×10^{-3} m/s

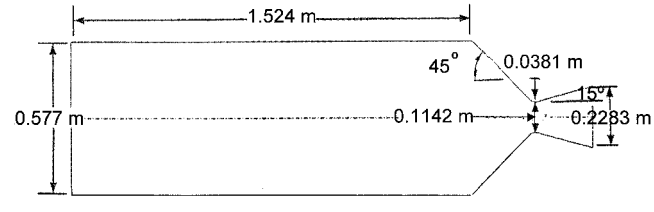

Fig. 1 Schematic of motor geometry.

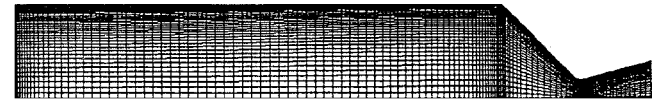

Fig. 2 Computational domain and grid.

distributed combustion on the flowfield, the calculations were performed with and without the distributed combustion model. The calculations with a surface combustion model assume complete combustion of the AP/binder and aluminum at the propellant surface. Chemical equilibrium calculations provide an adiabatic flame temperature of 3435.6 K for these conditions. The continuous-phase mass flux specified for these calculations included the aluminum mass and was adjusted to remove the mass corresponding to the caps. Following the data reported by Salita,[20] it was assumed that 20% of the aluminum in the propellant results in formation of Al_2O_3 caps due to surface oxidation, etc., whereas 80% Al_2O_3 was considered to be part of the continuous phase in the form of smoke.

For the distributed combustion calculations, it was assumed that none of the aluminum in the propellant reacts at the propellant surface. Hence, the specified continuous-phase mass flux was computed by excluding the aluminum mass from the propellant, and the aluminum mass fraction in the gas at the propellant surface was set to 0.0. All of the aluminum mass was injected in the form of droplets in the discrete phase. The temperature of the gas injected at the propellant surface was set to the adiabatic flame temperature for the propellant formulation exclusive of the aluminum. The heat required to melt the aluminum and raise it to the flame temperature was appropriately accounted for in the flame temperature calculations. The resulting flame temperature was 2592.5 K. Note that the assumption that no aluminum in the propellant reacts at the surface is not inherent to the formulation discussed here. This assumption was made in these calculations in the absence of any other information. If better information is available about what part of the aluminum in the propellant reacts at the surface, calculations can be performed with that information equally easily.

The code was run in the single-phase mode, that is, continuous phase only neglecting the effect of particulate phase, to establish the flowfield corresponding to propellant combustion exclusive of the aluminum. Subsequently, the injection of aluminum droplets at the propellant surface was initiated. The injected particles undergo combustion in accordance with the empirical model, thereby increasing the aluminum mass fraction in the continuous phase. The calculations have also assumed that 20% of the reacted aluminum is allocated to the discrete phase in the form of Al_2O_3 caps. Thus, the fractional mass of Al_2O_3 in the particles increases as the particle undergoes combustion. The discrete-phase analysis treats the composition of the particle as one of its attributes and, hence, can easily accommodate the composition change. Allocation of 20% Al_2O_3 to the discrete phase implies that $102/54 \times 0.2 \times 15\%$ of the propellant mass would be allocated to discrete phase on complete combustion of aluminum. Thus, complete combustion of the aluminum in the propellant would result in continuous-phase elemental aluminum mass fraction being $0.8 \times 15\%/(100 - 102/54 \times 0.2 \times 15) = 12.72\%$, most of which would be in the form of Al_2O_3 smoke in the continuous phase.

The results of the computations performed with the surface combustion assumption are compared with the results obtained using the distributed combustion model in Figs. 3–6. A comparison of the pressure contours obtained from the two calculations is presented in Fig. 3, which shows no significant differences. The temperature field predicted by the two calculations, however, are significantly different, as can be seen from Fig. 4. The surface combustion model predicts the temperature in the chamber to be fairly uniform at a value corresponding to the adiabatic flame temperature for this case

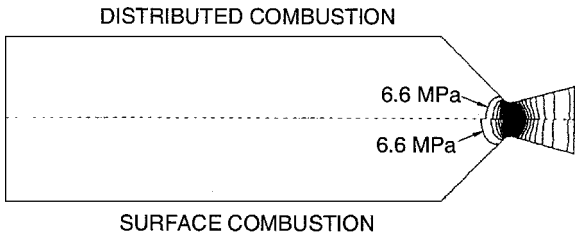

Fig. 3 Pressure contours: $P_{max} = 6.6$ MPa, $P_{min} = 0.4$ MPa, and $\Delta P = 0.2$ MPa.

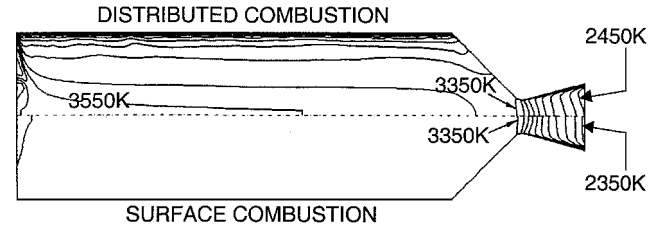

Fig. 4 Temperature contours: $T_{max} = 3750$ K, $T_{min} = 2350$ K, and $\Delta T = 100$ K.

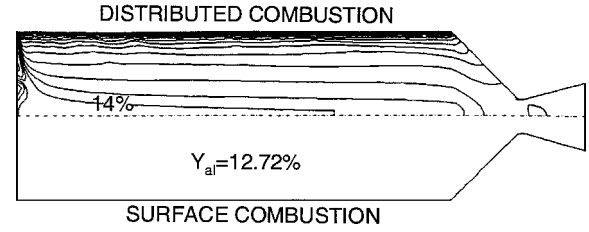

Fig. 5 Aluminum mass fraction contours: $Y_{max} = 17.0\%$, $Y_{min} = 0.0\%$ MPa, and $\Delta Y = 1.0\%$ MPa.

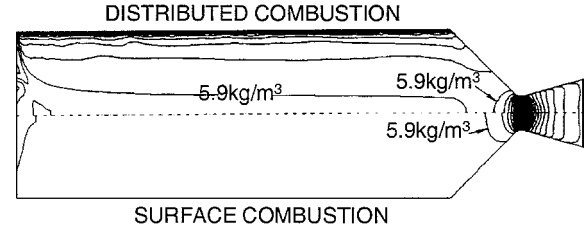

Fig. 6 Density contours: $\rho_{max} = 7.7$ kg/m^3, $\rho_{min} = 0.3$ kg/m^3, and $\Delta\rho = 0.2$ kg/m^3.

(3435.6 K). The distributed combustion calculations, however, show the chamber temperature to be quite nonuniform. The temperature at the propellant surface is 2592.5 K (the AP/binder flame temperature) and rises to about 3550 K in the core due to combustion of aluminum. As can be seen, the thermal boundary layer associated with this rise is approximately 20% of the chamber radius. There are indications that in the head end region the temperature is even higher. This is because the low velocities in this region do not allow the burning particles to be swept out and, hence, can result in local hot spots where some particles are present. These hot spots can also be observed in Fig. 5, where the contours of elemental aluminum mass fraction in the continuous phase have been plotted. The trapped particles result in the local elemental aluminum mass fraction exceeding 17% in this region. The elemental aluminum mass fraction in the core region of the chamber is about 14.0%. However, the mixing of the core flow with the gas near the propellant surface results in the elemental aluminum mass fraction near the nozzle exit being about 12.0%, indicating that only about 94.3%, (that is, $12/12.72 \times 100\%$) of the aluminum undergoes combustion in this motor. The continuous temperature at the nozzle exit is also seen to be about 100 K lower for the calculations performed using the distributed combustion model (compared with the surface combustion model calculations). This is consistent with reduced heat release in the motor chamber due to incomplete aluminum combustion.

The distributed combustion of aluminum also affects the continuous-phase density, and this effect can be seen in Fig. 6. The surface combustion assumption results in the gas density in the motor chamber being fairly uniform (approximately 6.0 kg/m^3), whereas the distributed combustion model results show the gas-phase density at the propellant surface being approximately 7.7 kg/m^3 and dropping to about 5.8 kg/m^3 in the core region due to the temperature rise caused by distributed combustion.

Following the coupled calculations to simulate the flowfield, isolated trajectory calculations were performed for particles injected at representative locations from the propellant surface. The trajectory calculations can be performed by specifying a large value for the

Lagrangian time step Δt_p so that the injected particle exits the computational domain. These calculations provide information about the particle residence time, the burn-up time, etc., for particles injected at various locations and a specified size. The results of these calculations indicate that the initial size of the injected particles has significant effect on aluminum combustion efficiency.

Summary

A two-phase, distributed combustion model to simulate the internal flow in solid rocket motors with metalized propellants is discussed. A Lagrangian analysis is used in this approach to simulate the discrete phase consisting of Al/Al_2O_3 particles. The combustion rate of these particles is assumed to be diffusion controlled and computed using empirical models. The continuous phase, consisting of combustion products from AP, binder, and the reacted aluminum, is analyzed using an Eulerian description. The kinetic timescales for reactions in the continuous phase are assumed to be very small, and tables generated using chemical equilibrium analysis have been used to reduce computational effort. The analysis incorporates full coupling between the two phases for mass, momentum, and energy exchange. The Eulerian–Lagrangian approach presented can also be easily adopted to study other significant phenomena in solid rocket motors, such as radiation effects and particle size changes due to agglomeration and breakup. Future research efforts should be directed in this direction because these effects can significantly affect the combustion process.

The results of the calculations demonstrate the ability of the analysis to simulate realistically the distributed combustion of aluminum in solid rocket motors. The calculations conducted with a propellant containing 15% aluminum indicate that the gas composition changes from its initial state (corresponding to AP/binder flame) to the final state (corresponding to peak elemental aluminum mass fraction) over an extended combustion region in the chamber. The chamber flowfield is not isothermal, as would be predicted if all of the aluminum were assumed to burn at the surface. Representative trajectory calculations were also performed, which provide useful information about the residence and burn-up times for selected particle sizes and injection locations.

The analysis discussed provides a more sophisticated tool for solid rocket internal flow predictions. This would not replace the simple and efficient correlations currently in use, but can be useful in studying apparent anomalies and improving the correlations. This analysis requires information regarding particle size distribution at the propellant surface, the fraction of metal that burns at the surface, etc. Further experiments aimed at collecting these data would be useful in validating the code. The code can also be used effectively in planning experiments, as well as interpreting the results from the experiments.

Acknowledgments

The analysis discussed here was developed by the author while employed at Scientific Research Associates, Inc. (SRA). The author would like to thank his colleagues at SRA who have made very significant contributions to this analysis. The author would also like to thank several other researchers in the field of solid rocket propulsion, particularly Jay N. Levine at the Air Force Research Laboratory/PRS for the numerous discussions, which have provided the much-needed insight during the development of this analysis.

References

[1]Culick, F. E. C., "Rotational Axisymmetric Mean Flow and Damping of Acoustic Waves in a Solid Propellant Rocket," *AIAA Journal*, Vol. 4, No. 8, 1966, pp. 1462–1469.

[2]Sabnis, J. S., Gibeling, H. J., and McDonald, H., "Navier–Stokes Analysis of Solid Propellant Rocket Motor Internal Flows," *Journal of Propulsion and Power*, Vol. 5, No. 6, 1989, pp. 657–664.

[3]Chang, I., "An efficient Solution for Viscous Flow Inside SRM," AIAA Paper 91-2429, June 1991.

[4]Madabhushi, R. K., Sabnis, J. S., de Jong, F. J., and Gibeling, H. J., "Calculation of Two-Phase Aft-Dome Flowfield in Solid Rocket Motors," *Journal of Propulsion and Power*, Vol. 7, No. 2, 1991, pp. 178–184.

[5]Golafshani, M., and Loh, H. T., "Computation of Two-Phase Viscous Flow in Solid Rocket Motors Using a Flux-Split Eulerian–Lagrangian Technique," AIAA Paper 89-2785, July 1989.

[6]Price, E. W., "Combustion of Metalized Propellants," *Fundamentals of Solid-Propellant Combustion*, edited by K. K. Kuo and M. Summerfield, Progress in Astronautics and Aeronautics, Vol. 90, AIAA, Washington, DC, 1984, pp. 479–513.

[7]Gough, P. S., "Numerical Analysis of a Two-Phase Flow with Explicit Internal Boundaries," U.S. Naval Ordnance Station, Rept. IHCR 77-5, Indian Head, MD, April 1977.

[8]Gibeling, H. J., McDonald, H., and Banks, N. E., "An Implicit Numerical Analyses for Two-Dimensional, Two Phase Turbulent Interior Ballistic Flows," AIAA Paper 84-0561, Jan. 1983.

[9]Crowe, C. T., Sharma, M. P., and Stock, D. E., "The Particle-Source-In Cell (PSI-CELL) Model for Gas Droplet Flows," *Journal of Fluids Engineering*, Vol. 99, 1977, pp. 325–332.

[10]Gosman, A. D., and Ioannides, E., "Aspects of Computer Simulation of Liquid-Fueled Combustors," *Journal of Energy*, Vol. 7, No. 6, 1983, pp. 482–490.

[11]Dukowicz, J. K., "A Particle–Fluid Model for Liquid Sprays," *Journal of Computational Physics*, Vol. 35, No. 2, 1980, pp. 229–253.

[12]Sabnis, J. S., Gibeling, H. J., and McDonald, H., "A Combined Eulerian–Lagrangian Analysis for Computation of Two-Phase Flows," AIAA Paper 87-1419, June 1987.

[13]Sabnis, J. S., de Jong, F. J., and Gibeling, H. J., "A Two-Phase Restricted Equilibrium Model for Combustion of Metalized Solid Propellants," AIAA Paper 92-3509, July 1992.

[14]Jones, W. P., and Launder, B. E., "The Prediction of Laminarization with a Two-Equation Model of Turbulence," *International Journal of Heat and Mass Transfer*, Vol. 15, 1972, pp. 301–314.

[15]Sabnis, J. S., Madabhushi, R. K., Gibeling, H. J., and McDonald, H., "On the Use of k–ε Turbulence Model for Computation of Solid Rocket Internal Flows," AIAA Paper 89-2558, July 1989.

[16]Gordon, S., and McBride, B. J., "Computer Program for Calculation of Complex Chemical Equilibrium Compositions, Rocket Performance, Incident and Reflected Shocks, and Chapman–Jouguet Detonations," NASA SP-273, Interim rev., March 1976.

[17]Briley, W. R., and McDonald, H., "Solution of the Multidimensional Compressible Navier–Stokes Equations by a Generalized Implicit Method," *Journal of Computational Physics*, Vol. 24, No. 4, 1977, pp. 372–397.

[18]Briley, W. R., Buggeln, R. C., and McDonald, H., "Solution of the Three-Dimensional Navier–Stokes Equations for a Steady Laminar Horseshoe Vortex Flow," AIAA Paper 85-1520-CP, June 1985.

[19]Bird, G. A., *Molecular Gas Dynamics*, Clarendon, Oxford, 1976.

[20]Salita, M., "Quench Bomb Investigation of Al_2O_3 Formation from Solid Rocket Propellants (Part II): Analysis of Data," 25th JANNAF Combustion Meeting, CPIA Publ. 498, Vol. I, Chemical Propulsion Information Agency, Laurel, MD, pp. 185–197.

[21]Clift, R., Grace, J. R., and Weber, M. E., *Bubbles, Drops and Particles*, Academic Press, New York, 1978.

[22]Kreith, F., *Principles of Heat Transfer*, Intext Educational, New York, 1973, p. 472.

[23]Hermsen, R. W., "Aluminum Combustion Efficiency in Solid Rocket Motors," AIAA Paper 81-0038, Jan. 1981.

[24]King, M. K., "Prediction of Metal Combustion Efficiency in Low Port-to-Throat Area Ratio and Nozzleless Solid Rocket Motors," AIAA Paper 82-1202, June 1982.

[25]Hunter, S. C., Cherry, S. S., Waldman, C. H., and Kliegel, J. R., "One Dimensional Reacting Three-Phase Flow with Mass Transfer Between Phases," Vol. i, Final TR AFRPL-TR-81-103, U.S. Air Force Rocket Propulsion Lab., April 1982.

[26]Bartlett, R. W., and Delaney, L. J., "Effect of Surface Tension on Maximum Particle Size in Two-Phase Nozzle Flow," *Pyrodynamics*, Vol. 4, 1966, pp. 337–341.

[27]Salita, M., "Use of Water and Mercury Droplets to Simulate Al_2O_3 Collision/Coalescence in Rocket Motors," *Journal of Propulsion and Power*, Vol. 7, No. 4, 1991, pp. 505–512.

[28]Abbas, A. S., Kousa, S. S., and Lockwood, F. C., "The Prediction of the Particle Laden Gas Flows," *Proceedings of the Eighteenth (International) Symposium on Combustion*, Combustion Inst., Waterloo, Canada, 1981, pp. 1427–1438.

[29]Hotchkiss, R. S., "The Numerical Modeling of Air Transport in Street Canyons," Rept. LA-UR-74-1427, Los Alamos Scientific Lab., Los Alamos, NM, 1974.